

DIFFUSION MODELING OF DECARBURIZATION MICROHARDNESS-DISTANCE PROFILES

Jürgen Gegner

SKF GmbH, Department of Material Physics
Ernst-Sachs-Strasse 5, D-97424 Schweinfurt, Germany
University of Siegen, Institute of Material Engineering
Paul-Bonatz-Strasse 9-11, D-57068 Siegen, Germany

ABSTRACT

Measured depth profiles of the microhardness are frequently used to estimate the carbon distribution in steels and, for instance, characterize the undesired heat treatment side effect of decarburization. For the quantitative evaluation of these graphs an analysis based on diffusion theory is often performed in the literature. The principal fundamentals and mathematical basics of this modeling technique are presented. If the relationship between hardness and carbon concentration is known, microhardness-distance curves of steels can be analyzed in this way. Mostly by implication, a linearized representation is assumed. This simple approximation is e.g. suitable for martensitically hardened grades in the concentration range from 0.15 to 0.6 m.% C. Microhardness depth profiles of steels with higher carbon content and other microstructures are also analyzed. The applicability of quantitative diffusion modeling is discussed in the present paper. Standard rolling bearing steel SAE 52100 (1.3505, German denotation: 100Cr6) serves as example material: microhardness-distance curves are measured for tempered and untempered martensitic and near-equilibrium microstructures of the alloy, which are further characterized by metallographic micrographs. The correlation to the carbon concentration and the X-ray diffraction line width is also considered.

INTRODUCTION

For the precise microchemical determination of carbon concentration-distance curves, a recently introduced method based on secondary ion mass spectrometry (SIMS) represents the best technique available today (1, 2). It is used in the present work. However, measuring carbon contents with such high accuracy and spatial resolution (e.g. by SIMS or electron microprobe analysis) is time-consuming and too expensive at least for routine laboratory investigations. Therefore, decarburization of steels is often examined on the etched metallographic cross section by visual microstructure evaluation in a light-optical microscope. Relevant features are, for instance, the martensite pattern and the carbide size. The metallographically determined decarburization depth, $dd_{(M)}$, is used in the literature to estimate the carbon diffusivity D_C (2-4):

$$D_C^{(M)} \approx \frac{dd_{(M)}^2}{t} \quad (1)$$

Here, t denotes the time of isothermal annealing. The superscript (M) indicates that this diffusion coefficient D_C is deduced metallographically. The X-ray diffraction (XRD) line broadening (full width at half maximum, *FWHM*) is also used to estimate the carbon profile of steels (5), since residual stresses of the third kind are a measure

of the lattice distortion. As concrete example, Fig. 1 reveals data for carburized case-hardening steel 17NiCrMo14 (1.3533): the line width of the $\{211\}$ ferrite reflection and the carbon content are plotted against the surface distance:

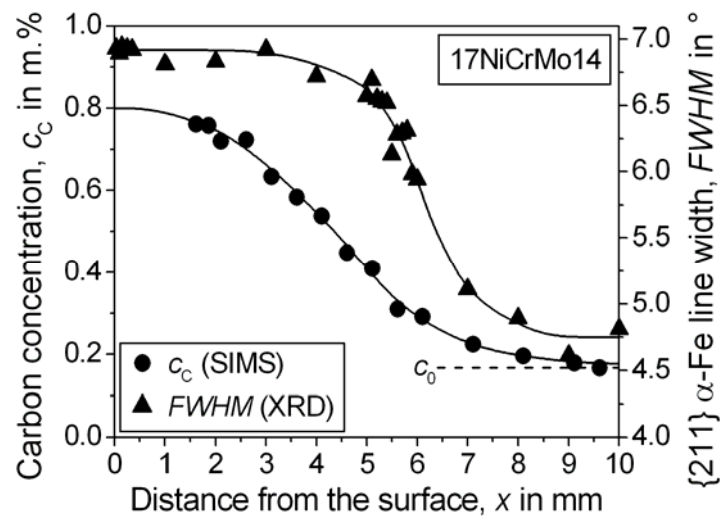


Fig. 1. Carburization profile (initial carbon concentration c_0) and XRD line width.

The resulting $FWHM-c_C$ relationship is presented in Fig. 2. The device-depending line width shows a sharp increase at lower carbon contents up to around 0.35 m.% C. Its maximum is reached at about 0.6 m.% C. However, the direct assignment of data, at least over a wider concentration range, is difficult and involves serious uncertainty. Diffusion modeling of line width depth profiles is discussed in the literature (2).

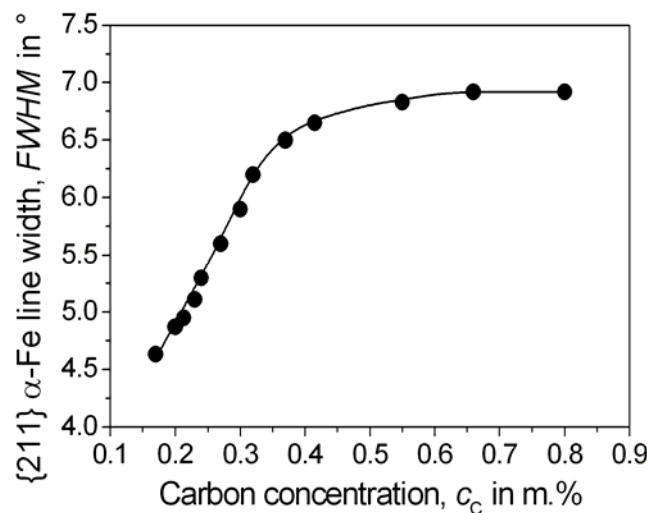


Fig. 2. $FWHM-c_C$ correlation derived from the two depth profiles in Fig. 1.

DIFFUSION ANALYSIS OF DECARBURIZATION MICROHARDNESS DEPTH PROFILES

Microhardness-distance curves are frequently measured to characterize the undesired steel heat treatment side effect of decarburization. Since metallography and XRD are approximate and time-consuming, respectively, this procedure represents the most important substitute technique amongst the indirect methods for the estimation of carbon

distributions and the strength of the effect of edge-zone material damage. Diffusion modeling is often used in the literature, even to derive the carbon diffusivity (3, 4), but mostly without explanation. If the relationship between hardness H and carbon concentration, which depends, amongst others, upon the grain size and the chemical composition of the steel, is a linear function with slope $a>0$ and intercept $b>0$

$$H = a \cdot c_C + b \Rightarrow c_C = \frac{H - b}{a} \quad (2)$$

the solutions of Fick's second law can be applied correspondingly. For tempered martensitic microstructures, for instance, this approximation holds in the range of carbon content from 0.15 to 0.6 m.%. The linear Hodge-Orehsoki hardenability relationship represents such an equation that is often successfully used in heat treatment practice of carburization (2, 6, 7): for 99.9 % martensite, $a=50$ HRC/m.% C and $b=(35\pm 2)$ HRC are derived. Analytical solutions for the isothermal decarburization diffusion problem are published elsewhere (2, 8). If constant surface carbon concentration c_s is assumed, the van Ostrand-Dewey equation is valid:

$$c_C = c_0 - (c_0 - c_s) \cdot \operatorname{erfc} \frac{x}{2\sqrt{D_C t}} \quad (3)$$

Substituting Eq. (2) into Eq. (3) by considering consistent subscripts for the surface (s) and the initial or core (0) values and simplifying the resulting expression yields:

$$H = H_0 - (H_0 - H_s) \cdot \operatorname{erfc} \frac{x}{2\sqrt{D_C t}} \quad (4)$$

Here, x , t , D_C and erfc denote the depth, time, carbon diffusivity and the error-function complement, respectively. This equation serves as the simplest basis for diffusion modeling of decarburization microhardness profiles and is used in the next section. If the boundary condition of constant surface carbon concentration is not met, however, more complex expressions must be applied. For instance, for a linear c_s decrease with time, i.e. $c_s=c_0-mt$ with slope $m>0$, the following transferred solution is valid (8):

$$H = H_0 - 4mt \left[\left(\frac{x^2}{8D_C t} - \frac{1}{4} \right) \operatorname{erfc} \frac{x}{2\sqrt{D_C t}} - \frac{x}{4\sqrt{\pi D_C t}} \exp \left(-\frac{x^2}{4D_C t} \right) \right] \quad (5)$$

A boundary condition of the third kind with the mass transfer coefficient β and the equilibrium (gas level) value $H_{\text{eq}}=H_s(t \rightarrow \infty)$ can be considered in the same way (2, 8):

$$H = H_0 - (H_0 - H_{\text{eq}}) \left[\operatorname{erfc} \frac{x}{2\sqrt{D_C t}} - \exp \left(\frac{\beta x + \beta^2 t}{D_C} \right) \operatorname{erfc} \left(\frac{x}{2\sqrt{D_C t}} + \beta \sqrt{\frac{t}{D_C}} \right) \right] \quad (6)$$

DECARBURIZATION OF ROLLING BEARING STEEL SAE 52100

Four examples for through-hardenable bearing steel SAE 52100 (German denotation 100Cr6) are presented. As far as known, Fig. 3 reveals the decarburization courses.

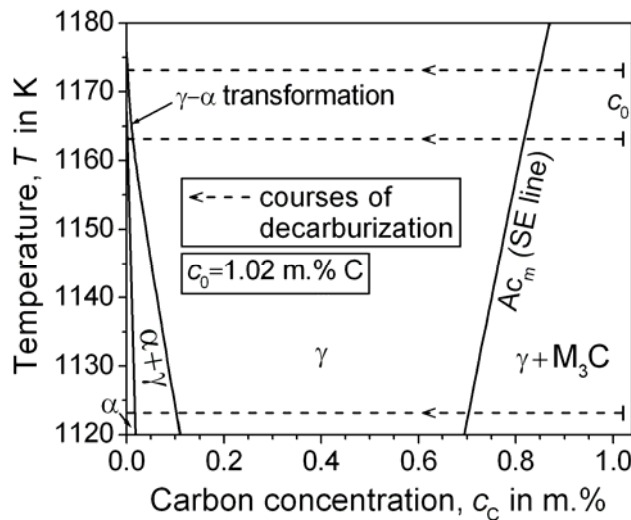


Fig. 3. Pseudo-phase diagram of SAE 52100 (Fe–Cr–C intersection at 1.5 m.% Cr).

Powder-Pack Decarburization

Two samples are annealed in an oxidizing Rhines-pack powder mixture, consisting of equal amounts of Fe_2O_3 , Fe and Al_2O_3 (the latter prevents the powder from adhering to the steel), for 5 h at 1123 and 1173 K, respectively. Light-optical micrographs of the etched cross-sections are given in Figs. 4 and 5:

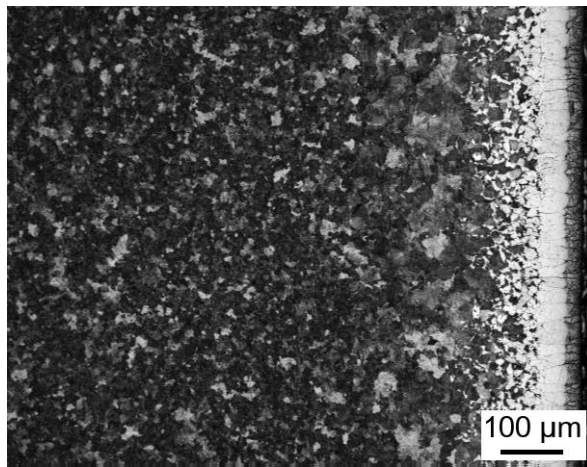


Fig. 4.

Near-surface microstructure of the 100Cr6 sample decarburized in Rhines pack at 1123 K for 5 h.

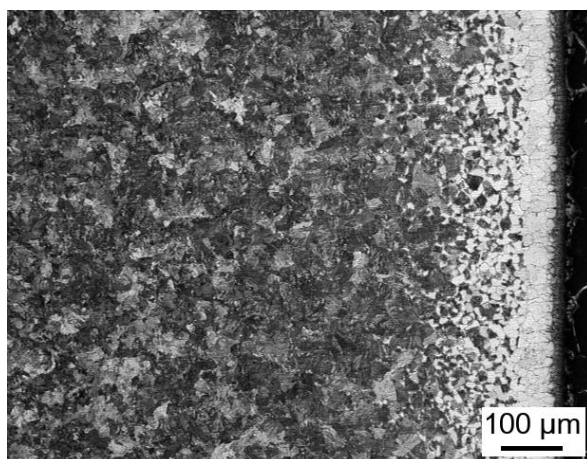


Fig. 5.

Near-surface microstructure of the 100Cr6 sample decarburized in Rhines pack at 1173 K for 5 h.

Since cooling of the samples after annealing occurs slowly in the surrounding argon atmosphere by removing the furnace from the quartz glass container, near-equilibrium ferritic-perlitic microstructures with rather low hardness are formed. As can be seen in Figs. 6 and 7, however, diffusion modeling of the Vickers microhardness profiles according to Eq. (4) results in good agreement of the fit curves with the measuring data in both cases. The Rhines-pack powder mixture leads to a very low surface concentration of carbon ($c_s \approx 0$) and thus an austenite-ferrite microstructure transformation in the edge zone (cf. Fig. 3). This effect, which particularly influences the depth profiles at 1123 K, is considered in the numerical analysis of the carbon concentration-distance curve that is also presented in Figs. 6 and 7. The core hardness is respectively reached in a depth that corresponds to around 0.6 to 0.7 m.% C. Due to the preserved carbide segregations, the SIMS data scatters more strongly in the c_C range to the right of the SE line in the phase diagram of Fig. 3. The carbon diffusivities in austenite derived by diffusion modeling from the microhardness and the concentration profile, $D_C^{(H)}$ and D_C , differ significantly from each other: as indicated in Figs. 6 and 7, the actual D_C values exceed $D_C^{(H)}$ by a factor of 4 to 5. This result is discussed later in the text.

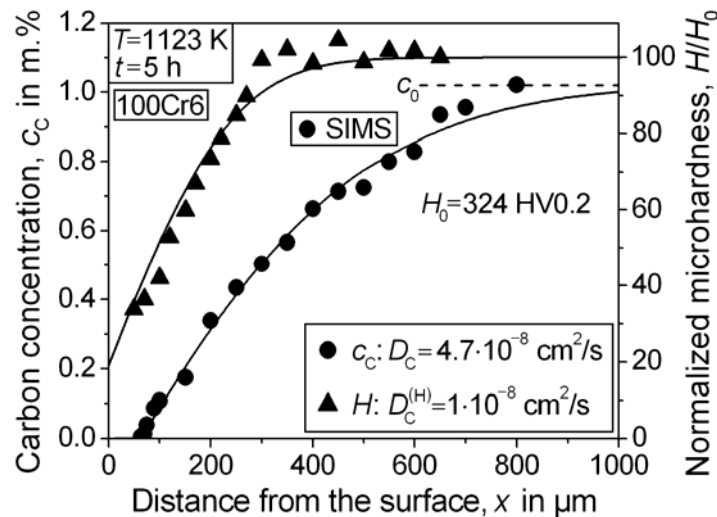


Fig. 6. Carbon and normalized microhardness profiles of the 1123 K sample.

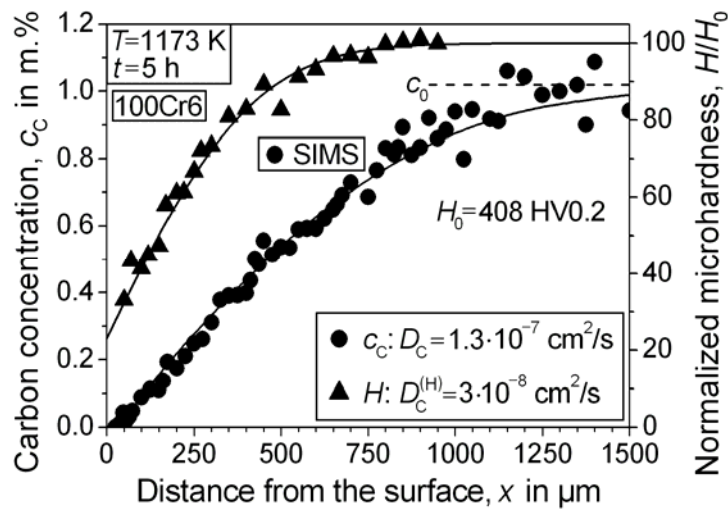


Fig. 7. Carbon and normalized microhardness profiles of the 1173 K sample.

Forging Defect

The next two examples of decarburization refer to martensitically hardened 100Cr6 steel. First, a forging defect is considered, which led to the failure of a bearing roller. Figure 8 shows the decarburized microstructure:

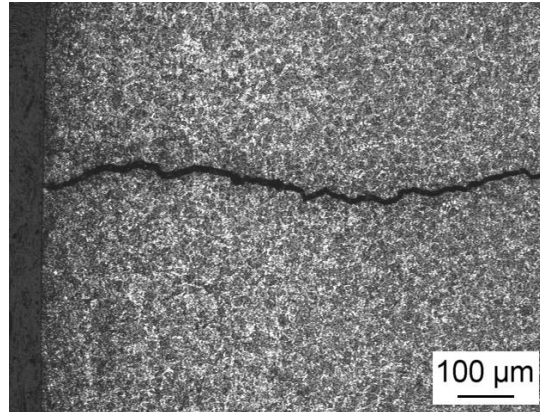


Fig. 8. Cross-sectional micrograph of a 100Cr6 bearing roller revealing a crack.

Carbon loss in the edge zone reduces the resulting hardness and causes tensile residual stresses in the near-surface region that support crack formation during operation under cyclic loading. In direct vicinity of the crack path shown in Fig. 8, the depth profiles of microhardness and carbon concentration are measured. Figure 9 gives the results:

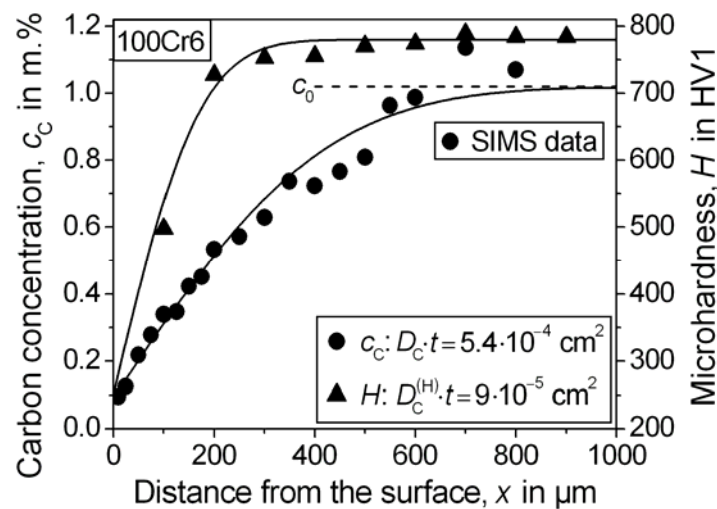


Fig. 9. Carbon- and microhardness-distance curve adjacent to the crack in Fig. 8.

The strong decarburization is too deep to be produced by austenitizing since this heat treatment process is performed between 1100 and 1170 K for around 30 min. The core hardness is virtually reached in a depth corresponding to 0.6 m.% C (see above). Diffusion modeling works for both measured profiles, as can also be seen in Fig. 9: the solid lines represent the best-fit curves according to Eqs. (3) and (4). As for this real failure case, the exact temperature and duration of decarburization are unknown, only the product of carbon diffusivity and time can be derived. The obtained values are indicated in the diagram and serve as a basis for the regarding t - T evaluation in Fig. 10.

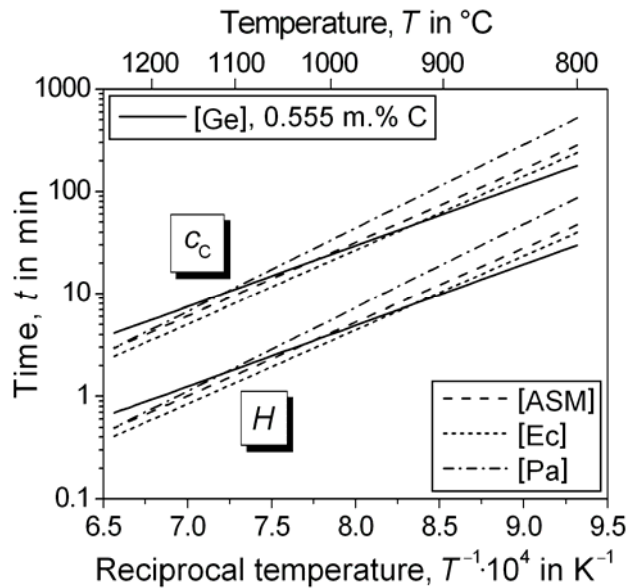


Fig. 10. Analysis of the data deduced from the depth profiles of carbon content and microhardness by diffusion modeling according to Eqs. (3) and (4) in Fig. 9. [ASM]: (11); [Ec]: (9); [Ge]: (12), at the concentration average; [Pa]: (10).

In this diagram, the time-temperature curves, which are obtained by substituting the stated literature references on the carbon diffusivity in austenite into the derived products of diffusion coefficient and time (cf. Fig. 9), are plotted. These graphs characterize the underlying decarburization process. Since $D_C = 6 \cdot D_C^{(H)}$ holds, this factor of 6 is translated into the corresponding sets of curves for the microhardness (H) and the carbon content (c_c) in Fig. 10. The realistic graphs derived from the concentration profile agree excellently with typical forging conditions, as this hot forming process occurs at temperatures around 1200 °C (1473 K) for times of a few minutes.

Purposely Produced Decarburization during Austenitizing

To study the effect of extreme decarburization during the austenitization process, an open out-diffusion anneal of a 100Cr6 sample in ambient air is performed at 1163 K for 30 min, after which the steel is martensitically hardened. Figure 11 reveals the resulting microstructure with damaged exfoliating scale at the surface (no blocking effect) and large ferrite containing areas (bright) in the edge zone:

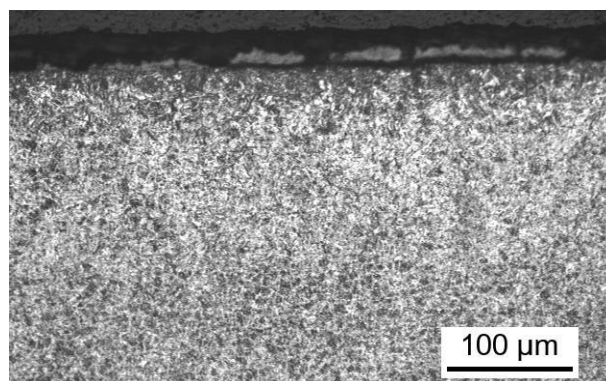


Fig. 11. Nital-etched microstructure of the strongly decarburized 100Cr6 specimen.

By applying Eq. (1), the rough metallographic analysis yields $dd_{(M)} \approx 150 \mu\text{m}$ and thus $D_C^{(M)} \approx 1.3 \cdot 10^{-7} \text{ cm}^2/\text{s}$ for the carbon diffusivity in the predominantly austenitic structure (cf. Fig. 3). Although the regarding decarburization depths dd differ considerably and the carbon distribution provides $dd \approx 350 \mu\text{m}$ (taken, by definition, at $c_C = 0.92 \cdot c_0$), this result is in good agreement with the outcome of diffusion modeling of the concentration profile also presented in Fig. 12; the applied fit equation is given elsewhere (8). The microhardness profile can be fitted very well by Eq. (4), which is consistently true for the untempered microstructure as shown in Fig. 13. The core values H_0 are respectively met in a depth that corresponds to a carbon content of around 0.6 m.%.

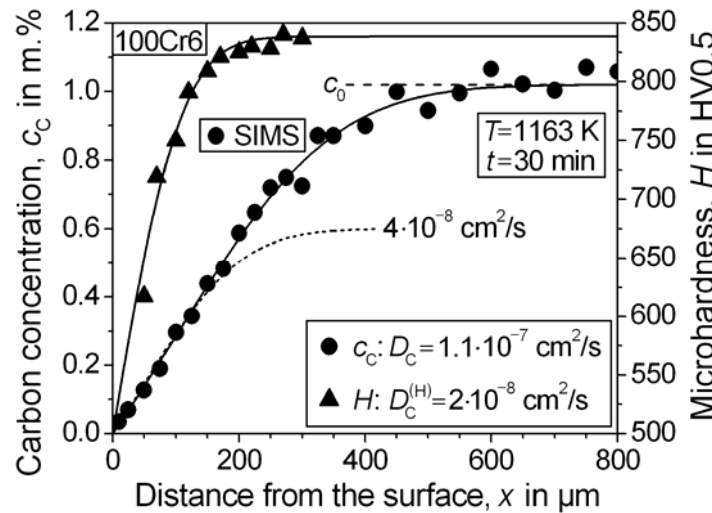


Fig. 12. Carbon concentration and microhardness depth profile in the tempered state.

The carbon diffusivities, which are derived from the microhardness- and the concentration-distance curve in Figs. 12 and 13 as fit parameters in the mathematical analysis, differ markedly from each other by a factor of 5.5: $D_C = 5.5 \cdot D_C^{(H)}$. Also the depth profile of the XRD line width is measured. The obtained result is given in Fig. 14. The differences of the values in the tempered and untempered state on the surface and in a depth of 10 μm point to microstructural constituents in addition to the ferrite grains.

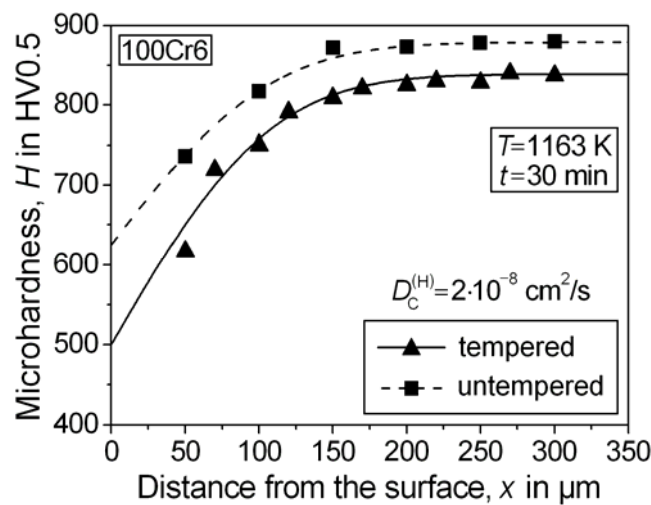


Fig. 13. Microhardness profiles measured in the tempered and untempered state.

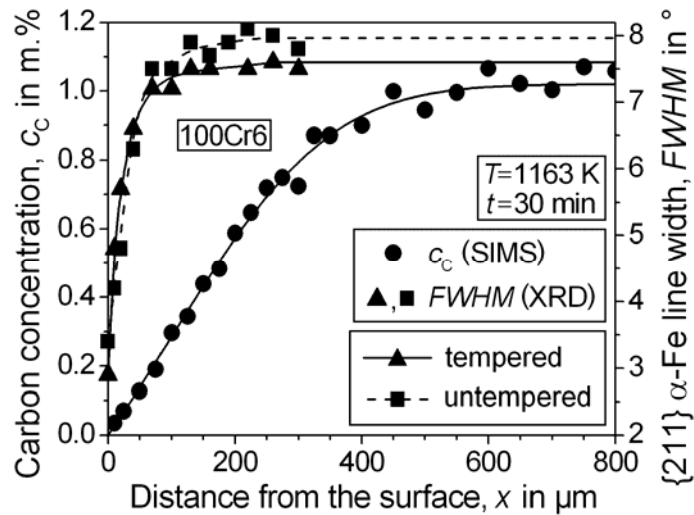


Fig. 14. Distance curves of the carbon concentration and the $\{211\}$ α -Fe line width.

From Fig. 14, the correlations between the line width and the carbon concentration are derived. Figure 15 shows the result for the tempered and untempered (only quenched) steel sample. These relationships can be compared with the curve in Fig. 2. Only up to carbon contents of 0.2 to maximal 0.3 m.%, a sufficiently sensitive correlation of both measuring quantities exists, which could allow for the direct extraction of the carbon concentration from the XRD line broadening.

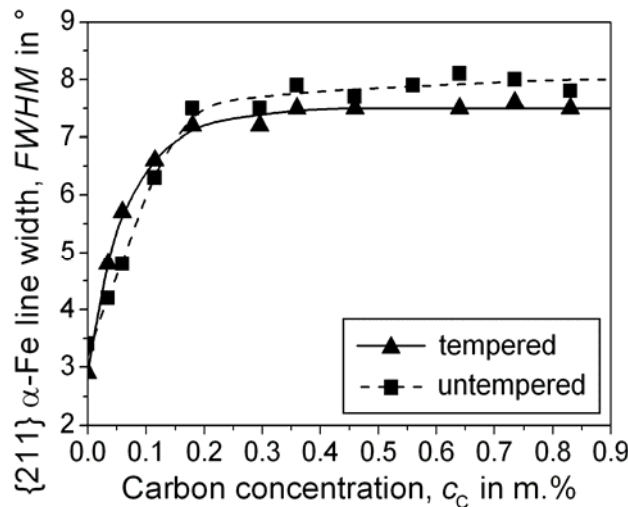


Fig. 15. $FWHM$ - c_C relationships according to Fig. 14.

DISCUSSION AND SUMMARY

The simplest method to estimate the carbon diffusivity from metallographically determined decarburization depths should only be used as a very rough approximation. In one of the presented examples, where it is tested, a rather good result for the diffusion coefficient of carbon in austenite is obtained by means of a decarburization depth that is evaluated much too small.

Decarburization microhardness-distance curves of through-hardenable 100Cr6 carbon steel can be fitted by diffusion modeling in good agreement with the measuring data.

In the present paper, this depth profile evaluation is performed for the martensitically hardened material and near-equilibrium ferritic-perlitic microstructures. However, the derived carbon diffusivities in the austenitic phase are found to be too low by a factor of around 5 and can thus not be rated capable of the description of carbon diffusion in austenitic 100Cr6 bearing steel. Values given in the literature [4], which are deduced from decarburization microhardness profiles for a high-carbon steel grade comparable with 100Cr6, lie in the same range from $2.6 \cdot 10^{-8}$ to $4.6 \cdot 10^{-8}$ cm²/s at 1123 to 1173 K. The reason for this deviation is that the fundamental linear relationship between hardness and carbon content is not valid over the whole concentration span. It holds, e.g., for martensite only up to maximum 0.6 m.% C: the carbon diffusion in the range of higher concentrations, which may be accompanied by carbide dissolution (8), cannot be followed by the profile of the hardness that remains almost constant, there. This restriction to lower and medium carbon contents evidently explains the underestimation of the diffusivity, which is illustrated in Fig. 12: the dotted curve represents a fit to the concentration data in this range with assumed initial content of 0.6 m.% C. The corresponding diffusivity of $4 \cdot 10^{-8}$ cm²/s is three times lower than for diffusion modeling of the whole carbon profile and close to the value derived from the microhardness.

REFERENCES

1. Wilbrandt P-J, Gegner J, Kirchheim R: 'Ein neues Messverfahren zur Bestimmung von Kohlenstoffprofilen'. HTM 2004 59 (4) 277-83.
2. Gegner J: Komplexe Diffusionsprozesse in Metallen. Renningen, expert Verlag, 2006.
3. Kučera J, Hajduga M, Glowacki J, Brož P: 'Decarburization and hardness changes of Fe-C-Cr-Mn-Si steels caused by high temperature oxidation in ambient air'. Z. Metallkd. 1999 90 (7) 514-21.
4. Adamaszek K, Bro P, Kučera J: 'Decarburization and hardness changes in carbon steels caused by high-temperature surface oxidation in ambient air'. Defect and Diffusion Forum 2001 194-199 1701-06.
5. Schreiber E: 'Umwandlungseigenspannungen'. HTM 1976 31 (1/2) 52-55.
6. Hodge J M, Orehoski M A: 'Relationship between Hardenability and Percentage of Martensite in Some Low Alloy Steels'. Trans. AIME 1946 167 627-42.
7. Schmidt P W: 'Zeit-Temperatur-Auflösungs- und Umwandlungs-Schaubilder'. Das Industrieblatt 1963 63 (6) 383-90.
8. Gegner J: 'Analytical modeling of carbon transport processes in heat treatment technology of steels'. 3rd Int Conf Mathematical Modeling and Computer Simulation of Materials Technologies, Ariel, College of Judea and Samaria, 2004, pp. 1/95-1/106.
9. Eckstein H-J: Wärmebehandlung von Stahl. Leipzig, VEB Verlag für Grundstoffindustrie, 1971.
10. Pavlossoglou J: 'Mathematische und Computer-Bestimmung der Gasaufkohlungsparameter – Kohlenstoffpotential, Kohlenstoffdiffusionskoeffizient und Reaktionsgeschwindigkeit'. HTM 1979 34 (1) 14-23.
11. Bardes B P (ed.): Metals Handbook. Vol. 4, Heat Treating. 9th ed., Metals Park (Ohio), American Society for Metals (ASM), 1981.
12. Gegner J: 'Concentration- and temperature-dependent diffusion coefficient of carbon in FCC iron mathematically derived from literature data'. 4th Int Conf Mathematical Modeling and Computer Simulation of Materials Technologies, Ariel, College of Judea and Samaria, 2006.